ARTICLE

Enhancement of Friction between Carbon Nanotubes: An Efficient Strategy to Strengthen Fibers

Xiaohua Zhang and Qingwen Li*

Suzhou Institute of Nano-Tech and Nano-Bionics, Ruoshui Road 398, Suzhou 215125, China

ABSTRACT Interfacial friction plays a crucial role in the mechanical properties of carbon nanotube based fibers, composites, and devices. Here we use molecular dynamics simulation to investigate the pressure effect on the friction within carbon nanotube bundles. It reveals that the intertube frictional force can be increased by a factor of 1.5−4, depending on tube chirality and radius, when all tubes collapse above a critical pressure and when the bundle remains collapsed with unloading down to atmospheric pressure. Furthermore, the overall cross-sectional area also decreases significantly for the collapsed structure, making the bundle stronger. Our study suggests a new and efficient way to reinforce nanotube fibers, possibly stronger than carbon fibers, for usage at ambient conditions.

KEYWORDS: molecular dynamics simulations · carbon nanotube bundles · structural transition · intertube friction · tensile strength

Carbon nanotubes (CNTs) are considered the strongest and ideal reinforcing fibers due to their exceptional mechanical properties, low density, and high aspect ratio. However, although the axial strength and stiffness of individual CNTs are of the order of 50−100 GPa and 1 TPa, respectively,[1−5] the highest strength of CNT and CNT-reinforced fibers, ranging from 0.85 to 3.3 GPa,[6−12] is nearly 2−3 orders of magnitude lower than individual tubes and about 1/3−1/2 of the strongest Toray carbon fibers.[13] As good alignment improves the translation of axial properties of individual tubes to those of the fiber, efforts were reported to grow ultralong and well-aligned CNT arrays (forests)[7] and to improve the direct spinning method.[10] Postspin treatments, such as infiltration, twisting, heating, and stretching, have been reported to improve the load transfer between CNT bundles, by making better oriented network[11] and closed packing[12] of bundles. However, CNTs often do not exist as individual tubes but group into bundles, the basic component of the spun fibers. Therefore, it can be of great importance to improve the strength of bundles. So far, the bundle strength is reported to be about 10 GPa for the length of several micrometers.[3] Considering the strength loss from component filaments to traditional fibers,[14] it is hard to achieve the same strength as carbon fibers by grouping CNT bundles through various spinning treatments. One problem strongly related to the bundle strength is that individual tubes in the bundle tend to slide easily against each other.[15] Recently, translational static and sliding frictions in a multiwall CNT were measured to be 0.014 and 0.009 meV/Å per atom, respectively,[16] and the frictional force in a bundle was reported, surprisingly, of several orders of magnitude greater,[17,18] due to different experimental conditions and probably also the existence of impurities. Although still hard to measure the friction between defect-free tubes, there is no doubt that, in order to achieve a strong bundle, tubes within it should be sufficiently long.

Here we show, from a series of molecular dynamics simulations, that prepressing on CNT bundles can greatly enhance intertube friction and consequently the strength of the nanotube fibers. The underlying mechanism involves the structural transition of CNTs, accompanied by an increase of intertube frictional force and the decrease of the cross-sectional area, as well. All tubes collapse above a critical pressure and remain collapsed after unloading, especially the large tubes. The friction increase, by a factor ranging from 1.5 to 4, is chirality dependent and is strongest for nonchiral tubes. Taking into account this new feature of prepressing, it might be possible to spin nanotube fibers stronger than carbon fibers under current spinning techniques. Furthermore, although strongly related to previ-

*Address correspondence to liqw05@gmail.com.

Received for review October 29, 2009 and accepted December 10, 2009.

Published online December 18, 2009. 10.1021/nn901515j

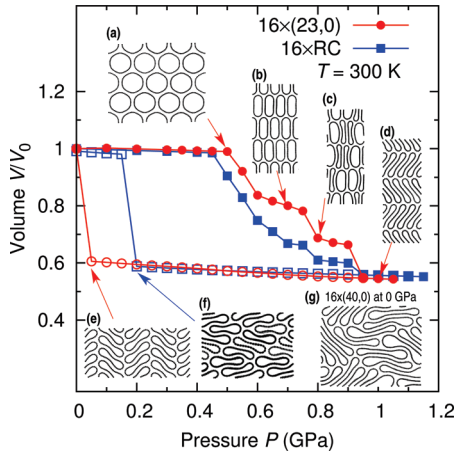

Figure 1. Volume *vs* pressure for the 16 × (23,0) and 16 × RC bundles. V_0 is the volume at zero pressure. The bundles show step-by-step structural transition, shown in filled circles and squares. By unloading the pressure (open circles and squares), the bundles remain collapsed until the return pressure below which the bundles expand to the initial structure. Insets a−d: Snapshots of the 16 × (23,0) bundle during the pressure loading up to 0.5, 0.7, 0.8, and 1.0 GPa, respectively. (e) Collapsed structure is remained when the 16 × (23,0) bundle is unloaded down to 0.05 GPa. (f) Collapsed 16 × RC bundle at 0.2 GPa. (g) Larger tubes as the 16 × (40,0) remain collapsed even under zero pressure. Here T = 300 K.

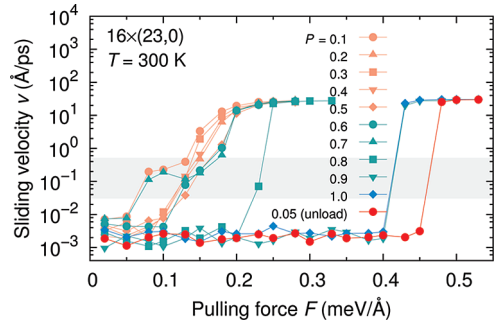

Figure 2. Sliding velocity of the sliding tube as a function of the pulling force F under different loadings for the 16 × (23,0) bundle. Speeds are all abstract values, and those smaller than 0.01 Å/ps are of the same magnitude of the error by averaging within finite time and thus correspond to zero velocity. Below the gray zone, the tube stays static, and above it, the tube slides at a speed plateau of 2600−3000 m/s, depending on the pressure.

ous studies on radial mechanical translation during the transition of individual CNTs or CNT bundles,[19−28] our study focusing on axial translation is obviously new and shows inspirational results.

RESULTS AND DISCUSSION

The simulation is set for defect-free single-wall CNT bundles which, named by tube number in the box and tube chirality, are 16 × (23,0), 16 × (40,0), and 16 × random chirality (RC), respectively. Figure 1 shows the volume−pressure (V−P) relation during the pressure loading up to 1.2 GPa and unloading down to 0 GPa for the 16 × (23,0) and 16 × RC bundles. The bundles show step-by-step structural transition. We define transition pressures P_t^{start} and P_t^{end} to denote the start and end of the transition zone. For the 16 × (23,0) P_t^{start} = 0.5 GPa and P_t^{end} = 0.95 GPa, and for the 16 × RC, they are 0.45 and 0.95 GPa, respectively. With unloading, all tubes remain collapsed until the return pressure P_r, 0.05 GPa for the 16 × (23,0) and 0.2 GPa for the other, below which each tube expands to the initial structure with big hollow space inside the tube. The transition pressures are almost the same because they are mainly radius-dependent,[22] while the return pressures are different due to the radius inhomogeneity. For bundles with large tube radius, for example, the 16 × (40,0) whose V−P curve is not shown here, P_t^{start} = 0.1 GPa, P_t^{end} = 0.35 GPa, and $P_r < 0$. Therefore, it is possible to get collapsed CNT bundles under atmospheric pressure. The clear experimental evidence of collapsed nanotubes was very recently reported by the Windle group[11] from the observation of the "dog-bone" cross section of double- and triple-wall nanotubes with equivalent diameter larger than ∼5 nm. It presents a possible way to improve the fibers during the direct spinning process, and it also will be of great importance to find a similar way for the spinning out of CNT forests. Insets a−e in Figure 1 show the structural changes during pressure loading and the unloaded structure for the 16 × (23,0) bundle. The unloaded 16 × RC and 16 × (40,0) bundles with collapsed tubes are shown in Figure 1 as insets f and g. The herringbone structure is obtained due to our large compression rate.[28]

As a model study, we fix one of the tubes and pull another as far as possible under an external pulling force F, along which we define the positive direction. We find, due to the strong commensurability of the 16 × (23,0) bundle, the tube under pulling does not slide until F is larger than the so-called depinning force f^{static} (static friction). Figure 2 shows the sliding velocity at different pulling forces, each value extracted from a simulation longer than 100 ps. Velocities smaller than 0.01 Å/ps, below the gray horizontal zone in Figure 2, are considered to be at rest because such values, either positive or negative, are within the systematic error due to the finite time average. The tube only slides when F goes beyond the pressure-dependent depinning force, which will be discussed below, and the tube speeds up, crosses the gray zone quickly, and finally slides at a speed plateau of 2600−3000 m/s due to phonon excitations. The speed plateau and its mechanism have been reported very recently[29,30] and are beyond the scope of the current study. Obviously, such huge sliding speed is unreal, and as a result, the bundle breaks due to the sliding. The sliding-induced breakage has already been observed as an abrupt diameter change in the tensile-loading experiment[3] and should be ubiquitous in fibers. Those speeds inside the gray zone in Figure 2 are actually unstable as we observed from simulation that the tube stops and slides intermittently. More interesting and important is f^{static} changes with loading. Before the transition, it is 0.1 meV/Å per atom and is in-

creased 4-fold when collapse happens. With unloading, f^{static} varies between 0.4 and 0.45 meV/Å, as the case under 0.05 GPa shown in Figure 2.

By considering the change of the cross-sectional area of different structures, one can estimate the increase of the tensile strength σ

$$\sigma = \sum f^{static}/A \quad (1)$$

where the summation is over all atoms of the tube under pulling and A is the total cross-sectional area divided by the tube number in the simulation box. This equation is valid because within the breaking strain (less than 10%) of CNT bundles[3] individual tubes show nearly longitudinal bond elongation rather than bond breaking and rotation and thus still have nearly the TPa stiffness.[5] It means that our assumption, that is, the summation of pulling forces is identical to the external load, is correct. When the load becomes larger than σ, it cannot be totally transferred to neighboring tubes as the sliding happens. Before the transition (*i.e.*, at 0.5 GPa), $A = 378$ Å^2 and $\sigma = 31.2$ MPa for the present simulation box length of about 34 Å. To reach the strength of 10 GPa, the bundle should be 1090 nm long, which agrees very well with the experiment,[3] and of the same order as a recent theoretical study.[31] Now, with prepressing to fully collapsed and with unloading down to 0.05 GPa, A reduces to 232 Å^2, σ is improved by $4 \times 1.63 = 6.52$ due to the quadruple increase of f^{static}, and the ratio 1.63 between area changes. Thus, the 10 GPa tensile strength can be achieved by a bundle longer than $1090/6.52 \approx 167$ nm because all of the load can be transferred between tubes.

One reason for the increase of friction is the larger tube−tube contact area for collapsed tubes. However, it is not enough to make the quadruple friction increase because the contact goes up much less than twice. To investigate the structural changes, we define the partial pair distribution function (PPDF)

$$g_\alpha(r) = \frac{V}{4\pi r^2 N_\alpha (N_{tot} - N_\alpha)} \sum_{i=1}^{N_\alpha} \sum_{\beta \neq \alpha} \sum_{j=1}^{N_\beta} \delta(r - |\vec{r}_i - \vec{r}_j|) \quad (2)$$

where α and β denote different tubes with atom numbers N_α and N_β, respectively, N_{tot} the total atom number, V the volume of simulation box, i and j the carbon atoms of tube α and β, and $\vec{r}_i - \vec{r}_j$ the displacement. The result, averaged among all tubes, is shown in Figure 3. The first distribution peak does not show clear changes before and after the structure transition (*i.e.*, from 0.5 to 1.0 GPa) because it reflects the averaged tube−tube distance of about 3.5 Å by using the current intertube potential. There are changes in the second peak, as its position shifts from $r = 4.45$ to 4.25 Å, and the strength drops greatly after the transition. Even with unloading, such changes still exist, except that all peaks become wider and the total PPDF curve becomes smoother. The third

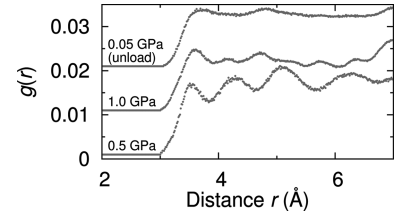

Figure 3. Partial pair distribution function $g(r)$ before nanotube collapse (0.5 GPa), after the collapse (1.0 GPa), and after the unloading (0.05 GPa) of the 16 × (23,0) bundle.

one around $r = 4.75$ Å at 1.0 GPa is a new peak and evidence of AB stacking between intertube graphite-like layers. Let us consider graphite structure and compare to the PPDF at 1.0 GPa. In the AB stacking with spacing h, the first-, second-, third-, and fourth-nearest distances from atoms of one layer to those of the other are h, $(h^2 + a^2)^{1/2}$, $(h^2 + 3a^2)^{1/2}$, and $(h^2 + 4a^2)^{1/2}$, respectively, where $a = 1.42$ Å is the C−C bond length. The number ratio between them is 1:9:6:9. Taking $h = 3.5$ Å from our simulation, one can find that the second-, third-, and fourth-nearest distances correspond exactly to the three PPDF peaks, respectively, with proper strengths. The nearest distance h is so close to the second one, with a small number ratio as well, that the h peak is overlapped, as shown in Figure 3. Here we just plot the PPDF for $r < 7$ Å in order to make clear the structural changes. If we extend the range to $r > 10$ Å, each PPDF curve reaches a constant that depends on the atom density. For example, the PPDF constant at 1.0 GPa is almost twice that at 0.5 GPa and slightly greater than the unloaded structure at 0.05 GPa.

The graphite-like structure of the collapsed CNT bundles can be also verified from calculations of the vibrational density of states (VDOS)

$$D_z(\omega) = \int e^{-i\omega t} \langle v_z(t) v_z(0) \rangle dt \quad (3)$$

where $D_z(\omega)$ denotes the VDOS along the z axis and $v_z(t)$ the velocity of atoms along z. Figure 4 shows the graphite-like modes before and after the transition and after unloading to 0.05 GPa. Three normal modes are la-

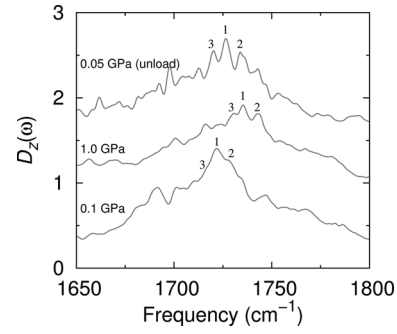

Figure 4. Vibrational density of states of the 16 × (23,0) bundle. Peaks numbered as 1, 2, and 3, for example, shift to higher energy after the transition (1.0 GPa) and after unloading to 0.05 GPa. These peaks are graphite-like modes, so the shift is larger at 1.0 GPa because the tube layers are more flattened. The energies are higher than the experimental values (about 1600 cm^{-1}) due to the current classical atomic potentials.

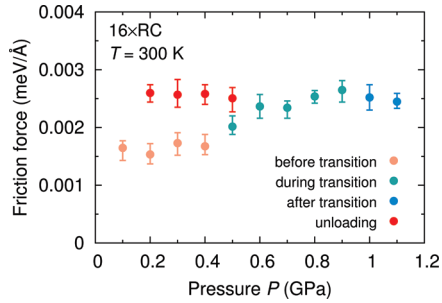

Figure 5. Sliding friction under different pressures for the 16 × RC bundle. Frictions are extracted from Newton's equation; see the text. Frictional force goes up by a factor of 1.5 when the transition happens and also after the unloading.

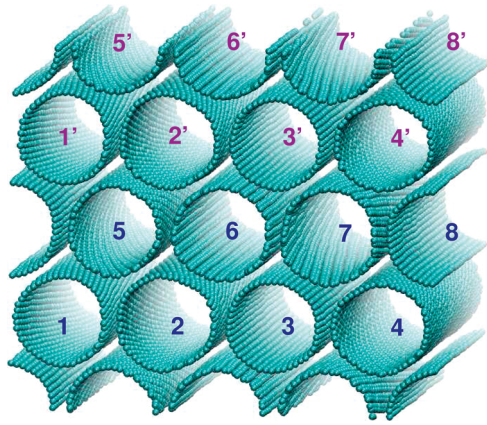

Figure 6. Tube arrangement of the 16 × RC bundle in the simulation box. Primed tubes are copies of those unprimed. Tube 1 is fixed to move, while tube 3′ is driven under an external pulling force acting on each atom. All other tubes are free to move.

beled to show the energy shift, which correspond to the G band shift that can be observed in experiments.[32,33] The shift is larger at 1.0 GPa because the tubes are more graphite-like, as shown in Figure 1. After the unloading, it is still detectable thus Raman scattering might be an efficient way to detect the tube collapse.

However, for the worst case of commensurability, the 16 × RC bundle, the intertube frictional force smaller than 0.002 meV/Å per carbon atom is about 2 orders of magnitude smaller, in agreement with experiments.[16,34] Furthermore, in our pulling simulation, it is the sliding friction rather than the depinning static force. However, we still find the prepressing also increases the sliding friction between tubes. The tube under pulling starts to move from the optimized structure when $F = 0.005$ meV/Å is applied, either in or out along the tube axis z. The friction f is extracted from Newton's equation when the sliding speed of that tube increases from 0 to around 1 Å/ps. For example, at 0.1 GPa, the speed goes up linearly from 0 to 0.8 Å/ps in 300 ps, corresponding to an acceleration of $a = 0.00267$ Å/ps^2. The sliding friction is $f = ma - F = -0.00168$ meV/Å, opposite to the pulling direction. However, after unloading to 0.2 GPa, it takes more than 420 ps to reach the speed of 0.8 Å/ps from 0, and the friction is extracted as −0.00263 meV/Å. In Figure 5, we plot the friction forces under different pressures where error bars indicate the friction fluctuation among several pulling simulations. Before the transition, frictional forces are all around 0.0017 meV/Å. It goes up greatly to 0.0026 meV/Å, by a factor of 1.5, when the transition happens. The friction value is maintained after the transition and also after the unloading. When the cross-sectional area changes are taken into account, the strength of a bundle composed of tubes with random chirality is almost tripled.

TABLE 1. Tube Chirality, Radius (R), Length (L), and Number of Atoms (N) in the Present Simulation (Note That L Changes Slightly in the Simulation Due to the Barostat)

tube	chirality	R (Å)	L (Å)	N
16 × (40,0): 1−8	(40,0)	15.66	21.30	800
16 × (23,0): 1−8	(23,0)	9.00	34.08	736
16 × RC: 1	(14,14)	9.49	104.00	2240
16 × RC: 2	(16,12)	9.52	104.00	2368
16 × RC: 3	(18,8)	9.03	104.00	2128
16 × RC: 4	(20,6)	9.23	104.00	2224
16 × RC: 5	(22,2)	9.03	104.00	2128
16 × RC: 6	(22,4)	9.49	104.00	2352
16 × RC: 7	(23,0)	9.00	104.00	2208
16 × RC: 8	(24,0)	9.39	104.00	2304

CONCLUSION

In summary, we have investigated the mechanical axial translation between nanotubes within CNT bundles. With a treatment of prepressing, the collapsed and compact structure is remained under a pressure as small as comparable to atmospheric pressure. After the collapse of tubes, not only does the cross-sectional area decrease but also the tube−tube frictional force goes up, especially by a factor of about 4 if the tubes are commensurate. Our study suggests a new and efficient way to reinforce the strength of CNT fibers, and actually, we have already been on the avenue of experimental studies.

METHODS

Periodic boundary conditions are used in all three dimensions. The tubes are initially assembled in hexagonal symmetry, with indexing numbers for the 16 × RC bundle shown in Figure 6, where primed tubes have the same chiralities as those unprimed. We list the chirality, radius, length, and atom number of each tube in Table 1. The length is sufficiently long to effectively reflect the energy transfer between tubes and to avoid the size effect where self-diffusion can be caused for short tubes due to the small energy variation between neighboring tubes. One constraint is used to fix the center of mass of tube 1 (see Figure 6), while tube 3′ is driven to move along tube axis z under an external pulling force F acting on each atom. We extract the static frictional force f^{static}, if possible, by assigning the critical pulling force below which no tube sliding happens and slides otherwise. The sliding frictional force f is extracted from the displacement−time curve of tube 3′ by using Newton's equation $F + f = ma$, m being the mass of carbon atom and a the overall acceleration along z. Temperature $T = 300$ K

and pressure are globally controlled by the Berendsen's algorithm.[35] We set along z zero pressure, $P_z = 0$, while the cross-sectional pressure $P_x = P_y$ varies between 0 and 1.2 GPa. The homogeneous isothermal compressibility in the cross-sectional plane is chosen to be 1 order of magnitude larger than that along z. The intratube C−C covalent bonds are described by the reactive empirical bond-order potential,[36] while the intertube van der Waals interactions and those between intratube non-neighbor atoms are described by a Lennard-Jones potential,[37] as our previous study has used.[22]

Acknowledgment. We acknowledge funding support from Chinese Academy of Science (hundred talent program and knowledge innovation program), and international collaboration project by Ministry of Science and Technology. We also thank Prof. Yuntian Zhu for instructive comments. Parts of the calculations were performed in the Shanghai Supercomputer Center (SSC) of China.

REFERENCES AND NOTES

1. Treacy, M. M. J.; Ebbesen, T. W.; Gibson, J. M. Exceptionally High Young's Modulus Observed for Individual Carbon Nanotubes. *Nature* **1996**, *381*, 678–680.
2. Lu, J. P. Elastic Properties of Carbon Nanotubes and Nanoropes. *Phys. Rev. Lett.* **1997**, *79*, 1297–1300.
3. Yu, M.-F.; Files, B. S.; Arepalli, S.; Ruoff, R. S. Tensile Loading of Ropes of Single Wall Carbon Nanotubes and Their Mechanical Properties. *Phys. Rev. Lett.* **2000**, *84*, 5552–5555.
4. Ruoff, R. S.; Qian, D.; Liu, W. K. Mechanical Properties of Carbon Nanotubes: Theoretical Predictions and Experimental Measurements. *C.R. Physique* **2003**, *4*, 993–1008.
5. Dumitrica, T.; Hua, M.; Yakobson, B. I. Symmetry-, Time-, and Temperature-Dependent Strength of Carbon Nanotubes. *Proc. Natl. Acad. Sci. U.S.A.* **2006**, *103*, 6105–6109.
6. Zhang, M.; Atkinson, K. R.; Baughman, R. H. Multifunctional Carbon Nanotube Yarns by Downsizing an Ancient Technology. *Science* **2004**, *306*, 1358–1361.
7. Li, Q.; Zhang, X.; DePaula, R. F.; Zheng, L.; Zhao, Y.; Stan, L.; Holesinger, T. G.; Arendt, P. N.; Peterson, D. E.; Zhu, Y. T. Sustained Growth of Ultralong Carbon Nanotube Arrays for Fiber Spinning. *Adv. Mater.* **2006**, *18*, 3160–3163.
8. Zhang, X.; Li, Q.; Tu, Y.; Li, Y.; Coulter, J. Y.; Zheng, L.; Zhao, Y.; Jia, Q.; Peterson, D. E.; Zhu, Y. Strong Carbon-Nanotube Fibers Spun from Long Carbon-Nanotube Arrays. *Small* **2007**, *3*, 244–248.
9. Zhang, X.; *et al.* Ultrastrong, Stiff, and Lightweight Carbon-Nanotube Fibers. *Adv. Mater.* **2007**, *19*, 4198–4201.
10. Motta, M.; Li, Y.-L.; Kinloch, I.; Windle, A. Mechanical Properties of Continuously Spun Fibers of Carbon Nanotubes. *Nano Lett.* **2005**, *5*, 1529–1533.
11. Motta, M.; Moisala, A.; Kinloch, I. A.; Windle, A. H. High Performance Fibres from 'Dog Bone' Carbon Nanotubes. *Adv. Mater.* **2007**, *19*, 3721–3726.
12. Tran, C. D.; Humphries, W.; Smith, S. M.; Huynh, C.; Lucas, S. Improving the Tensile Strength of Carbon Nanotube Spun Yarns Using a Modified Spinning Process. *Carbon* **2009**, *47*, 2662–2670.
13. The strongest high modulus and the highest tensile strength Toray carbon fibers have the strengths of 4.71 and 6.37 GPa, respectively. Toray Carbon Fibers America, Inc., http://www.toraycfa.com.
14. Hearle, J. W. S. The Structural Mechanics of Fibers. *J. Polym. Sci., Part C* **1967**, *20*, 215–251.
15. Salvetat, J.-P.; Briggs, G. A. D.; Bonard, J.-M.; Bacsa, R. R.; Kulik, A. J.; Stöckli, T.; Burnham, N. A.; Forrö, L. Elastic and Shear Moduli of Single-Walled Carbon Nanotube Ropes. *Phys. Rev. Lett.* **1999**, *82*, 944–947.
16. Cumings, J.; Zettl, A. Low-Friction Nanoscale Linear Bearing Realized from Multiwall Carbon Nanotubes. *Science* **2000**, *289*, 602–604.
17. Syue, S.-H.; Lu, S.-Y.; Hsu, W.-K.; Shih, H.-C. Internanotube Friction. *Appl. Phys. Lett.* **2006**, *89*, 163115.
18. Yang, T.; Zhou, Z.; Fan, H.; Liao, K. Experimental Estimation of Friction Energy within a Bundle of Single-Walled Carbon Nanotubes. *Appl. Phys. Lett.* **2008**, *93*, 041914.
19. Elliott, J. A.; Sandler, J. K. W.; Windle, A. H.; Young, R. J.; Shaffer, M. S. P. Collapse of Single-Wall Carbon Nanotubes Is Diameter Dependent. *Phys. Rev. Lett.* **2004**, *92*, 095501.
20. Zhang, X. H.; Liu, Z. F.; Gong, X. G. Comment on "Collapse of Single-Wall Carbon Nanotubes Is Diameter Dependent". *Phys. Rev. Lett.* **2004**, *93*, 149601.
21. Elliott, J. A.; Sandler, J. K. W.; Windle, A. H.; Young, R. J.; Shaffer, M. S. P. Reply to "Comment on 'Collapse of Single-Wall Carbon Nanotubes Is Diameter Dependent'". *Phys. Rev. Lett.* **2004**, *93*, 149602.
22. Zhang, X. H.; Sun, D. Y.; Liu, Z. F.; Gong, X. G. Structure and Phase Transitions of Single-Wall Carbon Nanotube Bundles under Hydrostatic Pressure. *Phys. Rev. B* **2004**, *70*, 035422.
23. Sun, D. Y.; Shu, D. J.; Ji, M.; Liu, F.; Wang, M.; Gong, X. G. Pressure-Induced Hard-to-Soft Transition of a Single Carbon Nanotube. *Phys. Rev. B* **2004**, *70*, 165417.
24. Ye, X.; Sun, D. Y.; Gong, X. G. Pressure-Induced Structural Transition of Double-Walled Carbon Nanotubes. *Phys. Rev. B* **2005**, *72*, 035454.
25. Gadagkar, V.; Maiti, P. K.; Lansac, Y.; Jagota, A.; Sood, A. K. Collapse of Double-Walled Carbon Nanotube Bundles under Hydrostatic Pressure. *Phys. Rev. B* **2006**, *73*, 085402.
26. Ye, X.; Sun, D. Y.; Gong, X. G. Molecular Dynamics Study of Radial Pressure Transmission in Multiwalled Carbon Nanotubes. *Phys. Rev. B* **2007**, *75*, 073406.
27. Zang, J.; Aldás-Palacios, O.; Liu, F. MD Simulation of Structural and Mechanical Transformation of Single-Walled Carbon Nanotubes under Pressure. *Commun. Comput. Phys.* **2007**, *2*, 451–465.
28. Shanavas, K. V.; Sharma, S. M. Molecular Dynamics Simulations of Phase Transitions in Argon-Filled Single-Walled Carbon Nanotube Bundles under High Pressure. *Phys. Rev. B* **2009**, *79*, 155425.
29. Zhang, X.-H.; Tartaglino, U.; Santoro, G. E.; Tosatti, E. Velocity Plateaus and Jumps in Carbon Nanotube Sliding. *Surf. Sci.* **2007**, *601*, 3693–3696.
30. Zhang, X. H.; Santoro, G. E.; Tartaglino, U.; Tosatti, E. Dynamical Chiral Symmetry Breaking in Sliding Nanotubes. *Phys. Rev. Lett.* **2009**, *102*, 125502.
31. Qian, D.; Liu, W. K.; Ruoff, R. S. Load Transfer Mechanism in Carbon Nanotube Ropes. *Compos. Sci. Technol.* **2003**, *63*, 1561–1569.
32. Venkateswaran, U. D.; Rao, A. M.; Richter, E.; Menon, M.; Rinzler, A.; Smalley, R. E.; Eklund, P. C. Probing the Single-Wall Carbon Nanotube Bundle: Raman Scattering under High Pressure. *Phys. Rev. B* **1999**, *59*, 10928–10934.
33. Peters, M. J.; McNeil, L. E.; Lu, J. P.; Kahn, D. Structural Phase Transition in Carbon Nanotube Bundles under Pressure. *Phys. Rev. B* **2000**, *61*, 5939–5944.
34. Dienwiebel, M.; Verhoeven, G. S.; Pradeep, N.; Frenken, J. W. M.; Heimberg, J. A.; Zandbergen, H. W. Superlubricity of Graphite. *Phys. Rev. Lett.* **2004**, *92*, 126101.
35. Berendsen, H. J. C.; Postma, J. P. M.; van Gunsteren, W. F.; DiNola, A.; Haak, J. R. Molecular Dynamics with Coupling to an External Bath. *J. Chem. Phys.* **1984**, *81*, 3684–3690.
36. Brenner, D. W.; Shenderova, O. A.; Harrison, J. A.; Stuart, S. J.; Ni, B.; Sinnott, S. B. A Second-Generation Reactive Empirical Bond Order (REBO) Potential Energy Expression for Hydrocarbons. *J. Phys.: Condens. Matter* **2002**, *14*, 783–802.
37. Mao, Z.; Garg, A.; Sinnott, S. B. Molecular Dynamics Simulations of the Filling and Decorating of Carbon Nanotubules. *Nanotechnology* **1999**, *10*, 273–277.